Biomedical engineering

Electric field induced in a spherical volume conductor from arbitrary coils: application to magnetic stimulation and MEG

H. Eaton

Johns Hopkins University Applied Physics Laboratory, Laurel, MD 20723, USA

Abstract—*A mathematical method is presented that allows fast and simple computation of the electric field and current density induced inside a homogeneous spherical volume conductor by current flowing in a coil. The total electric field inside the sphere is computed entirely from a set of line integrals performed along the coil current path. Coils of any closed shape are easily accommodated by the method. The technique can be applied to magnetic brain stimulation and to magnetoencephalography. For magnetic brain stimulation, the total electric field anywhere inside the head can be easily computed for any coil shape and placement. The reciprocity theorem may be applied so that the electric field represents the lead field of a magnetometer. The finite coil area and gradiometer loop spacing can be precisely accounted for without any surface integration by using this method. The theory shows that the steady-state, radially oriented induced electric field is zero everywhere inside the sphere for ramping coil current and highly attenuated for sinusoidal coil current. This allows the model to be extended to concentric spheres which have different electrical properties.*

Keywords—*Boundary value, Coil, Electric field, Induced field, Induction, Magnetic stimulation, MEG, Sphere, Volume conductor*

Med. & Biol. Eng. & Comput., 1992, **30**, 433–440

1 Introduction

MAGNETIC STIMULATION is a technique for noninvasive stimulation of nerve tissue. The brain can be stimulated through the intact head without causing pain (BARKER *et al.*, 1987) using magnetic stimulation. Magnetic stimulators presently have limited ability to confine the electric field to a small target region, and the precise site of stimulation is difficult to predict. To improve this situation, a detailed understanding of the induced electric field is a necessary first step.

The distribution of the electric field in the head induced by current flowing in a nearby coil can also be used to interpret magnetoencephalograms. Magnetoencephalography (MEG), like magnetic brain stimulation, also uses coils of wire located near the head as transducers. MEG is a technique for measuring the minute magnetic fields generated by brain activity. MEG can be used to precisely locate the source of brain activity, both evoked and spontaneous (WILLIAMSON and KAUFMAN, 1984).

Many investigators have modelled, in some way, the induced fields in the brain during magnetic stimulation. Some models have neglected the conductor boundary (COHEN, L. G. *et al.*, 1990), whereas others have treated it as an infinite conducting half space (TOFTS, 1990). More advanced models include a quasispherical volume analysed with finite-element techniques (UENO *et al.*, 1988) and a three-sphere model using a finite-difference approximation (ROTH *et al.*, 1991). All of these investigators provide results for specific coil shapes which have specific orientations to the head. In practical applications of magnetic brain stimulation, the desired coil shape and placement may not conform to any of these previously published cases. Several investigators have tried to determine experimentally how coil orientation affects brain stimulation (AMASSIAN *et al.*, 1989; COHEN, L. G. *et al.*, 1991; MEYER *et al.*, 1991; UENO *et al.*, 1990).

This paper presents a method for directly computing the total electric field inside a homogeneous spherical volume conductor for any practical excitation coil of any orientation. The method is simple and can provide highly accurate results with little computing time on a PC. The reciprocity theorem allows the results to be applied to MEG problems as well.

2 Model system

Fig. 1 shows the sphere model which is centred at the origin of the co-ordinate system. The sphere is assumed to have the permeability of free space μ_0, homogenous, isotropic conductivity σ_s and permittivity ε_s. Outside the

First received 17th June and in final form 20th September 1991

© IFMBE: 1992

sphere is free space ($\sigma = 0$, $\varepsilon = \varepsilon_0$). Above the sphere is an arbitrarily shaped excitation coil carrying a known current distribution. The current in the coil is assumed to flow in negligibly small filaments that are located at the centres of the wires; the theory can easily be expanded to include nonfilamentary coil currents. The frequency of excitation $\omega/2\pi$ is assumed to be low enough for all propagation effects and skin depth in the sphere to be neglected. These two approximations are valid as long as the coil is small

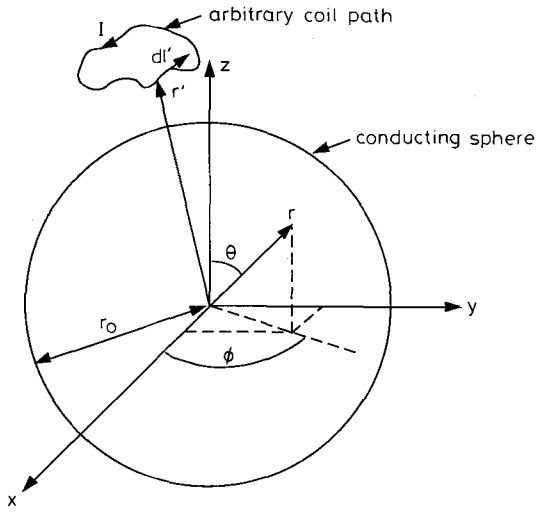

Fig. 1 *Co-ordinate system used in the model development. The spherical co-ordinate system and its relationship to the cartesian co-ordinates is shown. The vector* $\boldsymbol{r}$ *locates the point inside the sphere where the electric field is calculated. The vector* $\boldsymbol{r}'$ *points to the differential element of coil length being integrated. The differential vector* $\boldsymbol{dl}'$ *is tangent to the coil path at* $\boldsymbol{r}'$*. The coil must form a closed loop outside the sphere*

(not much larger than the head of radius r_0) and $\sqrt{\omega} \ll \sqrt{2/r_0^2 \mu_0 \sigma_s}$. For the human head, this approximation is valid up to about 500 kHz. This paper does not neglect the effects of the head capacitance. With skin depth neglected, the magnetic field arising from induced currents is ignored, so the total magnetic field is only the magnetic field produced by the excitation coil. All time varying signals are assumed to vary as $e^{j\omega t}$, where $j = \sqrt{-1}$. Alternatively, all field quantities can be thought of as Fourier transforms of the time domain quantities.

2.1 *Derivation of field equations*

The magnetic field, $\boldsymbol{B}$ can be found from the curl of a vector potential $\boldsymbol{A}$:

$$\boldsymbol{B} = \nabla \times \boldsymbol{A} \tag{1}$$

The magnetic vector potential of the coil is given by

$$\boldsymbol{A} = \frac{\mu_0}{4\pi} \oint_{\text{coil}} \frac{I\boldsymbol{dl}'}{|\boldsymbol{r} - \boldsymbol{r}'|} \tag{2}$$

where $\boldsymbol{r}$ is a vector from the origin to the point where the field is being computed, $\boldsymbol{r}'$ is a vector from the origin to the differential element of coil current, I is the coil current and $\boldsymbol{dl}'$ is directed along the current path. Eqn. 2 is really three equations, one for each component of $\boldsymbol{A}$. The three equations are independent only in rectangular co-ordinates. Eqn. 2 has identically zero divergence for any closed coil (JACKSON, 1975). Substituting eqn. 1 into the Faraday law gives

$$\nabla \times \boldsymbol{E} = -\frac{\partial \boldsymbol{B}}{\partial t} = -j\omega \boldsymbol{B} = -j\omega \nabla \times \boldsymbol{A} \tag{3}$$

Collecting terms gives

$$\nabla \times (\boldsymbol{E} + j\omega \boldsymbol{A}) = 0 \tag{4}$$

which implies that

$$\boldsymbol{E} = -j\omega \boldsymbol{A} - \nabla V \tag{5}$$

where V is the potential function resulting from charge accumulation at the sphere boundary. V must satisfy the Laplace equation. A general solution to the Laplace equation in spherical co-ordinates is (ARFKEN, 1985)

$$V = \sum_{l=0}^{\infty} \sum_{m=-l}^{l} (F_{lm} r^l + G_{lm} r^{-l-1}) Y_{lm}(\theta, \phi) \tag{6}$$

where $Y_{lm}(\theta, \phi)$ are spherical harmonic functions and F_{lm} and G_{lm} are complex constants. The potential inside the sphere V_i must be finite at the origin, which requires all the G_{lm} constants to be zero for V_i. The potential outside the sphere V_0 must vanish as $r \to \infty$ which requires all of the F_{lm} constants to be zero for V_0. The resulting expressions for V_i and V_0 are

$$V_i = \sum_{l=0}^{\infty} \sum_{m=-l}^{l} F_{lm} r^l Y_{lm}(\theta, \phi) \tag{7}$$

$$V_0 = \sum_{l=0}^{\infty} \sum_{m=-l}^{l} G_{lm} r^{-l-1} Y_{lm}(\theta, \phi) \tag{8}$$

The tangential components of ∇V must be continuous across the sphere boundary. This requires that

$$G_{lm} = F_{lm} r_0^{2l+1} \tag{9}$$

for all l, m. Continuity of the normal component of the induced current requires that (at $r = r_0$)

$$(\sigma_s + j\omega\varepsilon_s)\left(j\omega \boldsymbol{A} \cdot \hat{\boldsymbol{r}} + \sum_{l=0}^{\infty} \sum_{m=-l}^{l} l F_{lm} r_0^{l-1} Y_{lm}(\theta, \phi)\right)$$
$$= j\omega\varepsilon_0\left(j\omega \mathbf{A} \cdot \hat{\boldsymbol{r}} - \sum_{l=0}^{\infty} \sum_{m=-l}^{l} (l+1) G_{lm} r_0^{-l-2} Y_{lm}(\theta, \phi)\right) \tag{10}$$

Combining eqns. 9 and 10 and simplifying results in (at $r = r_0$)

$$\sum_{l=0}^{\infty} \sum_{m=-l}^{l} [l(\sigma_s + j\omega\varepsilon_s) + j\omega\varepsilon_0(l+1)]$$
$$\times F_{lm} r_0^{l-1} Y_{lm}(\theta, \phi) = -[\sigma_s + j\omega(\varepsilon_s - \varepsilon_0)] j\omega \boldsymbol{A} \cdot \hat{\boldsymbol{r}} \tag{11}$$

Eqn. 11 can be solved for F_{lm} by multiplying both sides by orthogonal spherical harmonics and integrating over the sphere surface. This could be carried out by computing $\boldsymbol{A}$ from eqn. 2 and numerically integrating over the surface; however, this is computationally intensive and difficult because of the double integration required. By manipulating eqn. 2 it is possible to find a direct expression for F_{lm}.

The expression $1/|\boldsymbol{r} - \boldsymbol{r}'|$ used in eqn. 2 can be written in terms of spherical harmonic functions (JACKSON, 1975):

$$\frac{1}{|\boldsymbol{r} - \boldsymbol{r}'|} = 4\pi \sum_{l=0}^{\infty} \sum_{m=-l}^{l} \times \left[\frac{r^l}{(2l+1) r'^{l+1}} Y_{lm}^*(\theta', \phi') Y_{lm}(\theta, \phi)\right] \tag{12}$$

where * means the complex conjugate. Eqn. 12 is valid for $r' > r$. Substituting eqn. 12 into eqn. 2 and pulling unprimed variables outside the integral gives

$$\boldsymbol{A} = \mu_0 I \sum_{l=0}^{\infty} \sum_{m=-l}^{l} r^l Y_{lm}(\theta, \phi) \oint_{\text{Coil}} \frac{Y_{lm}^*(\theta', \phi')}{(2l+1) r'^{l+1}} \boldsymbol{dl}' \tag{13}$$

The integral term in eqn. 13 is merely a set of complex vector constants for a given coil geometry and placement.

Providing a symbol for the vector constant

$$\boldsymbol{C}_{lm} = \oint_{\text{Coil}} \frac{Y^*_{lm}(\theta', \phi')}{(2l+1)r'^{l+1}}\, d\boldsymbol{l}' \tag{14}$$

helps simplify the expression for $\boldsymbol{A}$:

$$\boldsymbol{A} = \mu_0 I \sum_{l=0}^{\infty} \sum_{m=-l}^{l} r^l Y_{lm}(\theta, \phi)\boldsymbol{C}_{lm} \tag{15}$$

For the boundary condition (eqn. 11) it is necessary to find the component of $\boldsymbol{A}$ in the $\hat{r}$ direction. Eqn. 2 must be evaluated in rectangular components, and so the same is true for eqn. 14. For convenience, each rectangular component of $\boldsymbol{C}_{lm}$ is given a symbol:

$$\boldsymbol{C}_{lm} = C^x_{lm}\hat{i} + C^y_{lm}\hat{j} + C^z_{lm}\hat{k} \tag{16}$$

$\boldsymbol{C}_{lm} \cdot \hat{r}$ can then by written as

$$\boldsymbol{C}_{lm} \cdot \hat{r} = \left[\frac{C^x_{lm} - jC^y_{lm}}{2}\right] \sin\theta e^{j\phi} + \left[\frac{C^x_{lm} + jC^y_{lm}}{2}\right] \sin\theta e^{-j\phi} + C^z_{lm}\cos\theta \tag{17}$$

Creating new symbols for two of the expressions above simplifies the notation:

$$\boldsymbol{C}_{lm} \cdot \hat{r} = D_{lm} \sin\theta e^{j\phi} + E_{lm} \sin\theta e^{-j\phi} + C^z_{lm}\cos\theta \tag{18}$$

where D_{lm} and E_{lm} are given by direct comparison between eqns. 17 and 18. Combining eqns. 15 and 18 allows $\boldsymbol{A} \cdot \hat{r}$ to be written as

$$\boldsymbol{A} \cdot \hat{r} = \mu_0 I \sum_{l=0}^{\infty} \sum_{m=-l}^{l} r^l Y_{lm}(\theta, \phi) [D_{lm} \sin\theta e^{j\phi} + E_{lm} \sin\theta e^{-j\phi} + C^z_{lm}\cos\theta] \tag{19}$$

The recurrence relationships of spherical harmonic functions are (ARFKEN, 1985)

$$Y_{lm}(\theta, \phi)\cos\theta = \sqrt{\frac{(l-m+1)(l+m+1)}{(2l+1)(2l+3)}}\, Y_{l+1,m}(\theta, \phi) + \sqrt{\frac{(l-m)(l+m)}{(2l-1)(2l+1)}}\, Y_{l-1,m}(\theta, \phi) \tag{20}$$

$$Y_{lm}(\theta, \phi)\sin\theta e^{j\phi} = -\sqrt{\frac{(l+m+1)(l+m+2)}{(2l+1)(2l+3)}} \times Y_{l+1,m+1}(\theta, \phi) + \sqrt{\frac{(l-m)(l-m-1)}{(2l-1)(2l+1)}}\, Y_{l-1,m+1}(\theta, \phi) \tag{21}$$

$$Y_{lm}(\theta, \phi)\sin\theta e^{-j\phi} = \sqrt{\frac{(l-m+1)(l-m+2)}{(2l+1)(2l+3)}}\, Y_{l+1,m-1}(\theta, \phi) - \sqrt{\frac{(l+m)(l+m-1)}{(2l-1)(2l+1)}}\, Y_{l-1,m-1}(\theta, \phi) \tag{22}$$

When eqns. 20–22 are substituted into eqn. 19, the indices shifted and the range of summation adjusted appropriately (zero terms added and eliminated as necessary), eqn. 19 becomes

$$\boldsymbol{A} \cdot \hat{r} = \mu_0 I \sum_{l=1}^{\infty} \sum_{m=-l}^{l} r^{l-1} Y_{lm}(\theta, \phi) \times \left\{ - D_{l-1,m-1}\sqrt{\frac{(l+m-1)(l+m)}{(2l+1)(2l-1)}} + E_{l-1,m+1}\sqrt{\frac{(l-m-1)(l-m)}{(2l+1)(2l-1)}} + C^z_{l-1,m}\sqrt{\frac{(l-m)(l+m)}{(2l+1)(2l-1)}} \right\} + \mu_0 I \sum_{l=0}^{\infty} \sum_{m=-l}^{l} r^{l+1} Y_{lm}(\theta, \phi) \times \left\{ D_{l+1,m-1}\sqrt{\frac{(l-m+2)(l-m+1)}{(2l+1)(2l+3)}} - E_{l+1,m+1}\sqrt{\frac{(l+m+2)(l+m+1)}{(2l+1)(2l+3)}} + C^z_{l+1,m}\sqrt{\frac{(l-m+1)(l+m+1)}{(2l+1)(2l+3)}} \right\} \tag{23}$$

Eqn. 23 has two double summations, the first starting at $l = 1$ and the second starting at $l = 0$. The Appendix shows that the bracketed term in the second double summation is zero for all l, m. Combining eqns. 23 and 11 and using the orthogonality of spherical harmonic functions allows a direct determination of the expansion coefficient for V_i:

$$F_{lm} = \frac{-j\omega\mu_0 I[\sigma_s + j\omega(\varepsilon_s - \varepsilon_0)]}{l(\sigma_s + j\omega\varepsilon_s) + j\omega\varepsilon_0(l+1)} \times \left\{ - D_{l-1,m-1}\sqrt{\frac{(l+m-1)(l+m)}{(2l+1)(2l-1)}} + E_{l-1,m+1}\sqrt{\frac{(l-m-1)(l-m)}{(2l+1)(2l-1)}} + C^z_{l-1,m}\sqrt{\frac{(l-m)(l+m)}{(2l+1)(2l-1)}} \right\} \tag{24}$$

for $l > 0$ and $F_{00} = 0$.

The total electric field can be found anywhere inside the sphere by combining eqns. 5, 12 and 24:

$$\boldsymbol{E} \cdot \hat{r} = -\mu_0 I \sum_{l=1}^{N+1} \sum_{m=-l}^{l} \times \frac{(j\omega)^2\varepsilon_0(2l+1)}{j\omega(\varepsilon_s l + \varepsilon_0 l + \varepsilon_0) + l\sigma_s} r^{l-1} Y_{lm}(\theta, \phi) \times \left\{ - D_{l-1,m-1}\sqrt{\frac{(l+m-1)(l+m)}{(2l+1)(2l-1)}} + E_{l-1,m+1}\sqrt{\frac{(l-m-1)(l-m)}{(2l+1)(2l-1)}} + C^z_{l-1,m}\sqrt{\frac{(l-m)(l+m)}{(2l+1)(2l-1)}} \right\} \tag{25}$$

$$\boldsymbol{E} \cdot \hat{\boldsymbol{\phi}} = -j\omega\mu_0 I \sum_{l=0}^{N} \sum_{m=-l}^{l} j \times (D_{lm} e^{j\phi} - E_{lm} e^{-j\phi}) r^l Y_{lm}(\theta, \phi) - \sum_{l=1}^{N+1} \sum_{m=-l}^{l} F_{lm} \frac{jm}{\sin\theta} r^{l-1} Y_{lm}(\theta, \phi) \tag{26}$$

$$\boldsymbol{E} \cdot \hat{\boldsymbol{\theta}} = -j\omega\mu_0 I \sum_{l=0}^{N-1} \sum_{m=-l}^{l} \left\{ - C^z_{l+1,m-1}\right.$$

$$\times e^{-j\phi}\sqrt{\frac{(l-m+2)(l-m+1)}{(2l+1)(2l+3)}}$$

$$+\sqrt{\frac{(l-m+1)(l+m+1)}{(2l+1)(2l+3)}}$$

$$\times [D_{l+1,m}e^{j\phi}+E_{l+1,m}e^{-j\phi}]\Big\}r^{l+1}Y_{lm}(\theta,\phi)$$

$$-\sum_{l=1}^{N+1}\sum_{m=-l}^{l}\Big\{j\omega\mu_0 I\Big[C^z_{l-1,m-1}$$

$$\times e^{-j\phi}\sqrt{\frac{(l+m-1)(l+m)}{(2l-1)(2l+1)}}$$

$$+\sqrt{\frac{(l-m)(l+m)}{(2l-1)(2l+1)}}(D_{l-1,m}e^{j\phi}+E_{l-1,m}e^{-j\phi})\Big]$$

$$+\tfrac{1}{2}F_{l,m-1}e^{-j\phi}\sqrt{(l-m+1)(l+m)}$$

$$-\tfrac{1}{2}F_{l,m+1}$$

$$\times e^{j\phi}\sqrt{(l+m+1)(l-m)}\Big\}r^{l-1}Y_{lm}(\theta,\phi) \qquad (27)$$

Eqns. 25–27 are all Nth order approximations, and become exact as $N \to \infty$. The rate of convergence of the series depends on the shape and location of the coil(s) and the location where the field is being computed. Generally, convergence is slow when the coil is large and located near the sphere and the field point is located near a current carrying wire. Convergence is fast when the coil is small and located far from the sphere and the field point is deep in the sphere. Because magnetic stimulator coils are usually much larger than magnetometer coils, magnetic stimulation calculation will normally require a higher order approximation than MEG calculations if equal accuracy is required. Superconducting magnetometers also require a Dewar flask to hold the cooling fluid, and so their coils are located farther from the head than magnetic stimulator coils.

2.2 *Radial field component*

Eqn. 25 shows the frequency response characteristic for the radial component explicitly. Inspection of the frequency response characteristics reveals that the radial component of the induced field decays to zero very quickly (in about $5(\varepsilon_s + 2\varepsilon_0)/\sigma_s$ s) for a ramping coil current and has a highly attenuated steady-state value for quadratically increasing and sinusoidal coil currents. This is in agreement with the predictions of COHEN, D. and CUFFIN (1991) and BRANSTON and TOFTS (1991) who show that the steady-state radial electric field induced during magnetic stimulation is zero for any coil shape and orientation. For brain tissue at low frequency $\varepsilon_s \approx 13\,000\varepsilon_0$ and $\sigma_s \approx 0{\cdot}14\,\mathrm{S\,m^{-1}}$ (STOY *et al.*, 1982), so the transient lasts about $4{\cdot}2\,\mu$s. The two tangential components are nonzero at steady state for ramp current inputs. This shows that significant radially oriented electric fields are very difficult to induce in a uniform spherical conductor. Even when ε_s is large (such as in brain tissue or even water), which increases the time during which a transient radial electric field exists, the radial field is still much smaller than the tangential field. This can be seen by examining the frequency response of the F_{lm} coefficients (eqn. 24). When $\varepsilon_s \gg \varepsilon_0$, the pole in eqn. 24 is approximately cancelled by one of the zeros, so that the F_{lm} coefficients begin very near their steady-state values. Therefore, when $\varepsilon_s \gg \varepsilon_0$ none of the field components change much between the transient and steady-state periods.

For magnetic brain stimulation and MEG work, the radial component is so small compared with the tangential components that it can be considered to be zero. If the radial field is zero, then the sphere can be made of concentric shells having different electrical properties, and eqns. 25–27 will still be correct. This is true because the different shells will put additional boundary conditions only on the normal (radial) field component. Because this component is zero everywhere inside the head, the shell boundary conditions are already met by the single sphere model.

3 Application

The implementation of eqns. 25–27 is straightforward. First, the coil geometry is used to define the path and direction (cartesian component) used in eqn. 14. The C_{lm} coefficients are computed for all l values up to $l = N$. Next the D_{lm}, E_{lm} and F_{lm} coefficients are computed and stored. The F_{lm} terms must be determined up to $l = N + 1$. The integrals are easily evaluated numerically because only line integrals having no singularities are used. For large l the integrands can be highly oscillatory, which may require some care in the numerical integration procedure. Once all of these coefficients are determined, the sums given in eqns. 25–27 may be evaluated for any particular location (r, θ, ϕ) inside the sphere. Subroutines for computing spherical harmonic functions are given in PRESS *et al.* (1986).

3.1 *Application to magnetic brain stimulation*

Several contour plots of the magnitude of the electric field in various planes through a sphere excited by a 'butterfly' shaped coil are shown in Fig. 2. The sphere diameter is 18 cm, and the coil is made from two 5 cm diameter circular loops touching at one point so that the loop planes intersect to form a 140° angle. The coils carry currents in opposite directions and are located so that the bisector (of the 140° angle), passing through the point where the loops touch, also passes through the centre of the sphere. The point of the 'V' formed by the coils is closest to the sphere and is 0·4 cm above the sphere surface. The plots show the steady-state electric field produced by a $1\,\mathrm{A\,s^{-1}}$ current ramp in each loop. The magnitude of the electric field scales directly with the current ramping rate, so that a coil current of $100\,\mathrm{A\,\mu s^{-1}}$ would change the scale from $1\,\mathrm{nV\,m^{-1}}$ to $0{\cdot}1\,\mathrm{V\,m^{-1}}$. Note that for this example each loop has only 1 turn.

Fig. 2 shows that the electric field is strongest near the

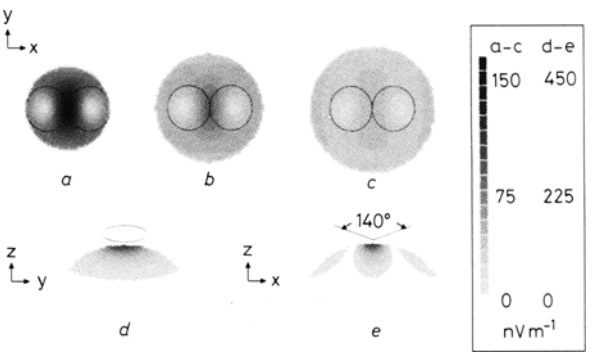

Fig. 2 *Magnitude of the steady-state electric field in a sphere model of the head produced by a 'butterfly' shaped coil carrying a current ramp of $1\,\mathrm{A\,s^{-1}}$. The sphere is centred at the origin and is 18 cm diameter. The coil has two loops 5 cm in diameter that touch on the z-axis to form a 140° angle. The butterfly 'body' is aligned along the y-axis 0·4 cm above the sphere surface. (a) The field in the planes $z = 7{\cdot}7$ cm; (b) $z = 6{\cdot}7$ cm; (c) $z = 5{\cdot}7$ cm; (d) $x = 0{\cdot}0$ cm; (e) $y = 0{\cdot}0$ cm*

coil and diminishes deeper in the sphere. There are two null points in the field which are near the projected loop centres in this example. The maximum electric field is located directly beneath the point where the loops adjoin. The field strength falls off rapidly with distance from the coil: the field strength near the brain surface ($z = 7{\cdot}7$ cm plane) is less than one-third of the value at the scalp surface.

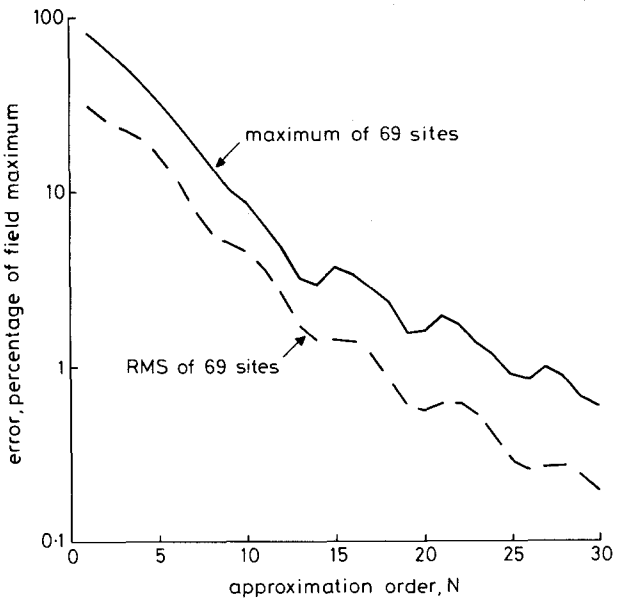

Fig. 3 *Convergence of the series solution of the vector potential. The magnitudes of the maximum and RMS vector error as a percentage of the maximum magnitude found in the plane are plotted against approximation order. Accuracy was checked at 69 points uniformly distributed in the plane $z = 7{\cdot}7$ cm (a region of slow convergence) for the butterfly coil used in Fig. 2. Undulations are an artefact of the computation at discrete points*

A twentieth order ($N = 20$) approximation was used to generate Fig. 2. The convergence characteristics for this coil were checked by comparing the vector potential computed by eqn. 15 (summed up to $l = N$) with an exact expression given in terms of complete elliptic integrals (JACKSON, 1975). The maximum vector error in A between the two methods (considering only θ and ϕ components) was 1·6 per cent of the maximum magnitude (as given by the exact expression) in the $z = 7{\cdot}7$ cm plane. Fig. 3 shows the convergence characteristics for this coil as the approximation order increases. The equations for A and E must converge at the same rate because of the relationship between $\boldsymbol{E} \cdot \hat{r}$ and the F_{lm} coefficients. The contour integrals were computed using an 80-point Gauss-Legendre integration formula (ABRAMOWITZ and STEGUN, 1964) for each loop. All the coefficients were computed on a Macintosh IIx (16 MHz 68882) in approximately 5 min. The low-order coefficients are given in Table 1. The coil symmetry yields all pure imaginary numbers for the tabulated coefficients. The C^y_{lm} coefficients were purely real, but not tabulated. Computing the field at 50 points took an additional

Table 1 First several constants characterising sphere/butterfly coil of Fig. 2

l	m	D	E	C^z	F
0	0	$-j0{\cdot}0257$	$j0{\cdot}0257$	0	0
1	0	$-j0{\cdot}3120$	$j0{\cdot}3120$	0	0
1	1	0	0	$j0{\cdot}1257$	$-j0{\cdot}0210$
2	0	$-j3{\cdot}639$	$j3{\cdot}639$	0	0
2	1	0	0	$j1{\cdot}517$	$-j0{\cdot}1268$
2	2	$-j0{\cdot}0900$	$-j0{\cdot}7271$	0	0
3	0	$-j39{\cdot}74$	$j39{\cdot}74$	0	0
3	1	0	0	$j16{\cdot}05$	$-j0{\cdot}894$
3	2	$-j1{\cdot}744$	$-j11{\cdot}62$	0	0
3	3	0	0	$j0{\cdot}4987$	$-j0{\cdot}0278$

All constant have units of m^{-l} except F which has units of $V m^{l}$. Coefficients for negative m can be determined from the relationships: $D_{l,-m} = (-1)^m E^*_{l,m}$; $E_{l,-m} = (-1)^m D^*_{l,m}$; $F_{l,-m} = (-1)^m F^*_{l,m}$; and $C^z_{l,-m} = (-1)^m C^{z*}_{l,m}$ where * means complex conjugate.

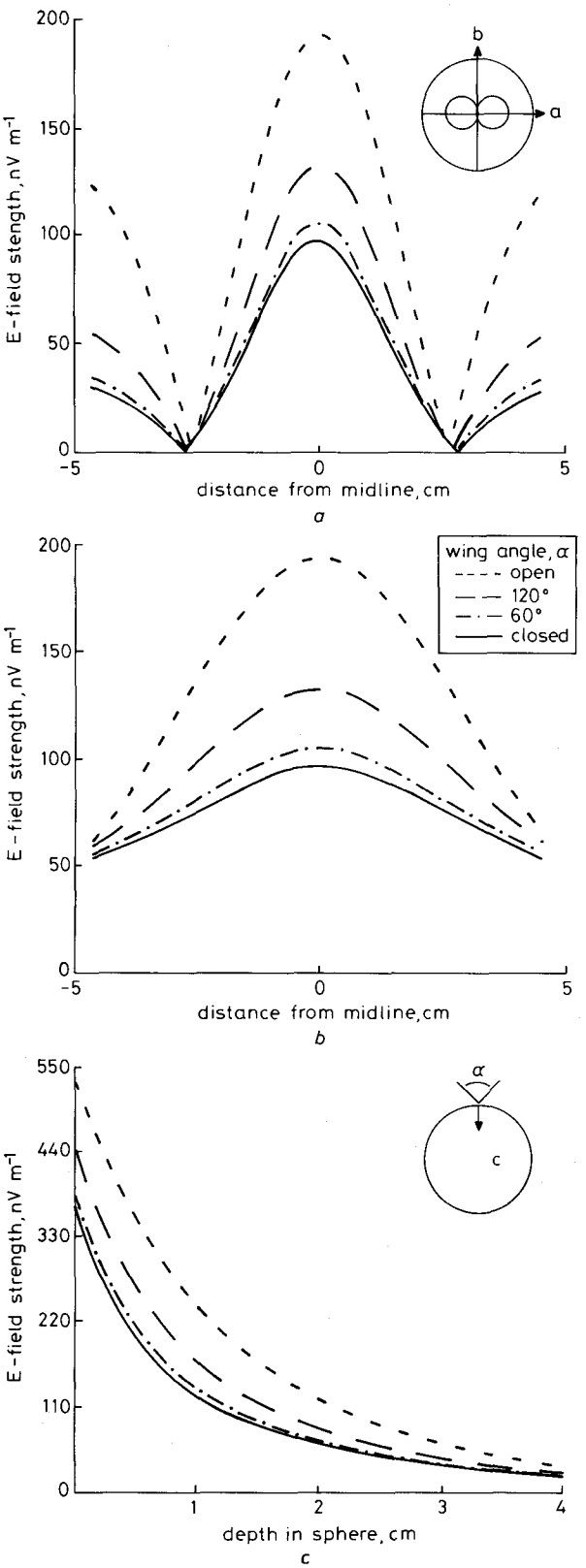

Fig. 4 *Electric field magnitude produced by butterfly coils having various 'wing' angles excited with a current ramp of $1\,A\,s^{-1}$. (a) Field strength along path a in a plane 1·3 cm below the sphere surface; (b) field strength along the path b in a plane 1·3 cm below the sphere surface; (c) field strength directly beneath the touching point of the loops against depth in the sphere*

30·9 s. No attempt was made to optimise the speed of the field computation. Speeding the field computation would be simple for this example because a large number of coefficients are equal to zero and the nonzero coefficients are all purely imaginary numbers.

The effect of changing the angle between the 'wings' of the 'butterfly' shaped coil on the induced field is shown in Fig. 4. The figure shows the magnitude of the electric field along two lines in the $z = 7{\cdot}7$ cm plane: one along the 'body' direction and one from 'wing-to-wing'. The two lines intersect directly beneath the point where the coil loops touch. These curves graphically illustrate how localised the electric field magnitude is. The full width at half maximum along the 'wing-to-wing' direction is 2·9 cm with the 'wings' closed and 3·2 cm with the 'wings' open. Along the 'body' direction the full width at half maximum is 10·3 cm with the 'wings' closed and 7·1 cm with the 'wings' open. As the field is broadest along the 'body' direction in both cases, the flat figure eight coil is most focal. The flat coil also produces the greatest field strength in the sphere. The rate at which the electric field diminishes with depth is similar for different 'wing' angles (Fig. 4*c*).

3.2 *Application to MEG*

The reciprocity theorem as developed by PLONSEY (1972) allows eqns. 25–27 to be interpreted as the lead field of an MEG magnetometer. For a SQUID magnetometer, the flux coupling the pick-up coil is a more useful quantity than the open-circuit coil voltage developed by Plonsey. Fortunately, a very simple relationship exists between the two. For a current dipole inside the sphere, the flux ϕ coupling the magnetometer pick-up coil is given by

$$\phi = -\frac{\boldsymbol{P} \cdot \boldsymbol{E}(\boldsymbol{r})}{j\omega I} \tag{28}$$

where $\boldsymbol{E}(\boldsymbol{r})$ is given by eqns. 25–27, $\boldsymbol{P}$ is the current dipole moment and $\boldsymbol{r}$ is the location of the dipole in the sphere. The coefficients used in eqns. 25–27 must be found from contour integrals following the path of the pick-up coil winding(s). Eqn. 28 provides a very convenient way to calculate the magnetometer response due to a current dipole inside a sphere (or concentric spheres) model. The contour integrations need only be carried out once to establish the geometric relationship between the sphere and pick-up coil, after which the flux from any current dipole located anywhere in the sphere with any orientation can be found. It should be noted that eqn. 28 computes the total flux seen by the coil accounting for the finite area of the coil, the loop spacing, winding direction and all 'secondary' sources arising from the sphere boundary, regardless of coil orientation.

Conventional MEG theory provides expressions for the magnetic fields produced by a given source distribution, rather than the flux through a coil. CUFFIN and COHEN, D. (1983) have shown that the finite area and gradiometer loop spacing significantly impact dipole parameter estimation if the magnetometers are assumed to measure the magnetic field at one point in space. Using a conventional magnetic field calculation from a dipole-sphere model (CUFFIN and COHEN, D., 1977) requires co-ordinate transformations and surface integration over the coil area(s) to accurately determine the theoretical flux. This is in comparison to eqn. 28 which only requires the evaluation of simple sums. Frequently in MEG, measurements are made at several sites to locate the equivalent dipole source. The localisation algorithm must find five parameters of the equivalent dipole. For a given location, the 'best' dipole moment in eqn. 28 can be determined by a linear least-squares process, so that the nonlinear optimisation algorithm need only search in a three-dimensional space. This can drastically reduce computation time compared with searching in a five-dimensional space.

An example of the response of a first-order gradient magnetometer to dipoles in a sphere is presented in Fig. 5. The magnetic field from a sphere 18 cm in diameter centred at the origin is measured by a magnetometer aligned parallel to the z-axis. The magnetometer has six

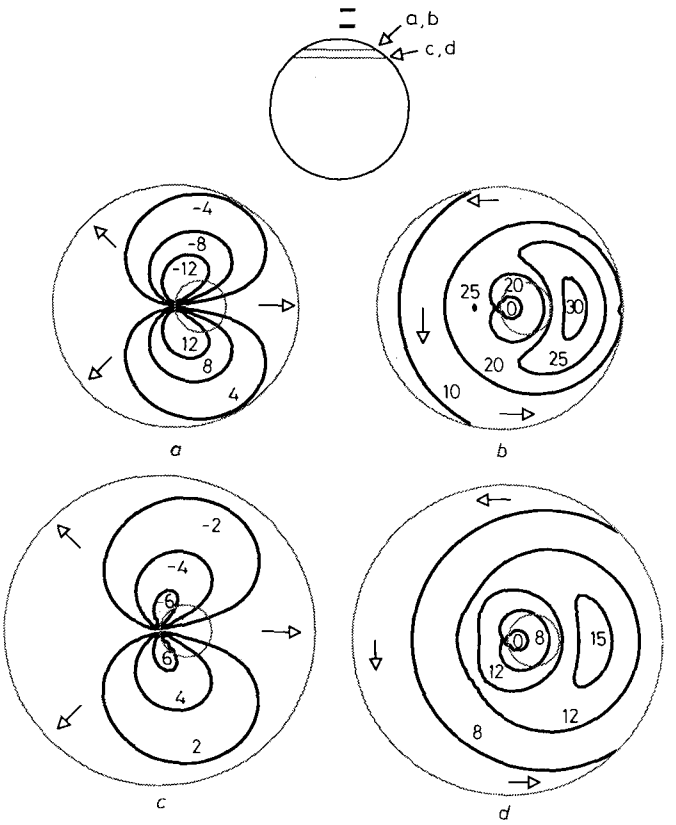

Fig. 5 *Contours of constant magnetomer flux (labelled in nWb $A^{-1} m^{-1}$) for various dipoles in an 18 cm diameter sphere. A first-order gradiometer (baseline of 2·0 cm) with six windings 2·0 cm in diameter is located parallel to the z-axis, 1·0 cm right of centre and 1·5 cm above the sphere surface. (a) The flux from dipoles oriented in the $\hat{\theta}$ direction; (b) the $\hat{\phi}$ direction in a plane 1·3 cm beneath the sphere surface; (c) $\hat{\theta}$ directed dipoles; (d) $\hat{\phi}$ directed dipoles in a plane 2·3 cm beneath the sphere surface. A 1 A m current dipole oriented in the $\hat{\theta}$ direction located anywhere on the contour labelled 12 in (a) will produce of flux of 12 nWb in the pick-up coil. Arrows indicate the $\hat{\theta}$ and $\hat{\phi}$ directions. The circles outlined in light grey show the projection of the magnetometer coil into the plane*

coaxial loops, 2 cm in diameter with centres on the line $y = 0$, $x = 1$ cm, all connected in series. The loops are located in planes of constant z at $z = 1{\cdot}5$ cm, 1·6 cm, 1·7 cm, 2·5 cm, 2·6 cm and 2·7 cm. The first three are wound in an anticlockwise direction and the last three in a clockwise direction viewed from above. Contours of constant pick-up coil flux are plotted in Fig. 5 for dipoles located in the $z = 7{\cdot}7$ cm plane (near the brain surface) and the $z = 6{\cdot}7$ cm plane having $\hat{\theta}$ or $\hat{\phi}$ orientations.

4 Discussion

Presently, the relationship between the applied field and resulting neural excitation in the brain is not well understood. Nerve fibres that are modelled as long and straight have been shown to be excited at a point where the electric field gradient along the fibre direction is maximum (ROTH

and BASSER, 1990), but models of finite-length fibres show that excitation occurs at the fibre terminus for a uniform field directed along the fibre length (REILLY, 1989). The later model may be more realistic for the complex geometry of neurons in the brain. This suggests that the site of maximum electric field oriented parallel to a nerve fibre may be the expected site of stimulation, which tends to agree with the experimental results of UENO (1990).

Many studies of the electric field produced by magnetic stimulator coils have examined the electric field in an air medium or an unbounded conducting medium without considering boundary conditions. The electric field in air produced by a 'butterfly' coil with various wing angles was examined by COHEN, L. G. *et al.* (1990). They concluded that with the 'wings' closed, the electric field was more focal and had similar magnitude to that with the 'wings' open but that the field direction was substantially different. These conclusions are correct in the absence of boundary conditions. When exciting a spherical volume conductor, however, opposite conclusions are reached (Fig. 4). The direction of the induced electric field does not change much between open and closed 'wing' positions, but the magnitude of the electric field is smaller and less focal with the 'wings' closed than with the 'wings' open. This example demonstrates the importance of considering the conductor boundary in the field calculation.

Knowing the electric field distribution during magnetic stimulation is important to understanding what structures in the brain may be stimulated. COHEN, D. and CUFFIN (1991) have suggested using the reciprocity theorem in conjunction with MEG theory to compute the electric field in the brain during magnetic stimulation. This approach requires integration of a complicated function over a surface bounded by the coil for each point where the field is to be found. Such an approach will be slow and difficult because of the two-dimensional integrations involved. Conversely, the application of reciprocity to the results of this paper yields a technique that could probably speed computations normally used in MEG dipole localisation. This may be particularly true for modern magnetometer arrays which are planar and therefore measure significant tangential magnetic flux. With enhanced speed, it may be possible to analyse the vast temporal data that are normally obtained during MEG experiments.

Fast calculation of eqn. 28 is desirable for an MEG source localisation algorithm. The speed of computation realised in this paper can be significantly improved by using a Shanks transform (SINGH *et al.*, 1990) on the l summations of eqns. 26–27. The Shanks transform allows $\boldsymbol{E}$ to be calculated accurately with only a few terms (small N). For example, for the butterfly coil used in Fig. 2, the same accuracy was achieved with 63 per cent less computer time when $N = 11$ with a twice iterated Shanks transform as when $N = 20$ without the Shanks transform. For coaxial circular coils located on one side of the head, such as those typically used in MEG work, the coefficients of large $|m|$ are insignificant, so considerable computer time may be saved by reducing the limits of the m summation for large values of l. Many other techniques may also help evaluate eqns. 26–27 faster. IOANNIDES and SWITHENBY (1987) have also suggested a series expansion that transforms the surface integration of the field over the coil area normally used in MEG computations into contour integration around the coil. Their technique has rapid convergence and applies to any head geometry, but requires volume integration of the current density everywhere in the head. Incorporating the dipole-in-a-sphere model with their technique would reduce the volume integration to surface integration of all 'secondary' sources arising from the sphere boundary. This seems to negate the advantages of their series expansion for simple geometric models.

The model for the head used in this paper has many shortcomings. Human heads are not spherical and are certainly far from having homogeneous, isotropic electrical properties, even when accounting for the gross inhomogeneities of skull and scalp layers. Nonetheless, a homogeneous sphere model is a good first approximation and has provided many useful results in MEG. The location of current sources artificially implanted in human brains have been accurately determined using MEG theory based on a homogeneous spherical head model (COHEN, D. *et al.* 1990). This suggests that the sphere model of the head is not bad for use in MEG. Because the magnetic fields produced by sources in the brain and electric fields induced in the brain by magnetic fields are reciprocal problems, the sphere model must also be reasonable for magnetic stimulation calculations even though no induced electric fields have been measured in actual human heads.

A wide variety of models for the head have been used for computing the induced electric field in the brain during magnetic stimulation. Many of these models used gross simplification of the head geometry to reduce the computational burden. The spherical shell model is arguably the best model with simple geometry. The sphere model also has indirect experimental verification from MEG experiments. This paper provides a simple and direct expression for the total electric field induced in the head from an arbitrary stimulator coil. Using this method, the field can be quickly computed with a personal computer. This should allow experimenters to correlate accurately the fields produced by the actual coils and placements they use with the physiological responses obtained. This is the first step to understanding how the induced electric field relates to the structures which are stimulated.

Acknowledgment—This work was supported by the US Navy under contract N00039-89-C-0001.

References

ABRAMOWITZ, M. and STEGUN, I. A. (1964) *Handbook of mathematical functions.* Dover Publications, New York.

AMASSIAN, V. E., CRACCO, R. Q., and MACCABEE, P. J. (1989) Focal stimulation of human cerebral cortex with the magnetic coil: a comparison with electrical stimulation. *Electroenceph. Clin. Neurophysiol.*, **74,** 401–416.

ARFKEN, G. (1985) *Mathematical methods for physicists.* Academic Press, Orlando, Florida.

BARKER, A. T., FREESTON, I. L., JALINOUS, R. and JARRATT, J. A. (1987) Magnetic stimulation of the human brain and peripheral nervous system: an introduction and the results of an initial clinical evaluation. *Neurosurg.*, **20,** 100–109.

BRANSTON, N. M. and TOFTS, P. S. (1991) Analysis of the distribution of currents induced by a changing magnetic field in a volume conductor. *Phys. in Med. & Biol.*, **36,** 161–168.

COHEN, D., CUFFIN, B. N., YUNOKUCHI, K., MANIEWSKI, R., PURCELL, C., COSGROVE, G. R., IVES, J., KENNEDY, J. G. and SCHOMER, D. L. (1990) MEG versus EEG localization test using implanted sources in the human brain. *Ann. Neurol.* **28,** 811–817.

COHEN, D. and CUFFIN, B. N. (1991) Developing a more focal magnetic stimulator. Part I: Some basic principles. *J. Clin. Neurophysiol.*, **8,** 102–111.

COHEN, L. G., ROTH, B. J., NILSSON, J., DANG, N., PANIZZA, M., BANDINELLI, S., FRIAUF, W. and HALLETT, M. (1990) Effects of coil design on delivery of focal magnetic stimulation. Technical considerations. *Electroenceph. Clin. Neurophysiol.*, **75,** 350–357.

COHEN, L. G., ROTH, B. J., WASSERMANN, E. M., TOPKA, H., FUHR, P., SCHULTZ, J. and HALLETT, M. (1991) Magnetic stimulation of the human cerebral cortex, an indicator of reorganization in motor pathways in certain pathological conditions. *J. Clin. Neurophys.*, **8,** 56–65.

CUFFIN, B. N. and COHEN, D. (1977) Magnetic fields of a dipole in special volume conductor shapes. *IEEE Trans.*, **BME-24,** 372–381.

CUFFIN, B. N. and COHEN, D. (1983) Effects of detector coil size and configuration on measurements of the magnetoencephalogram. *J. Appl. Phys.*, **54,** 3589–3594.

IOANNIDES, A. A. and SWITHENBY, S. J. (1987) An efficient magnetic flux integration method for bounded current sources. *Ibid.*, **61,** 4925–4927.

JACKSON, J. D. (1975) *Classical electrodynamics.* John Wiley & Sons, New York.

MEYER, B. U., BRITTON, T. C., KLOTEN, H., STEINMETZ, H. and BENECKE, R. (1991) Coil placement in magnetic brain stimulation related to skull and brain anatomy. *Electroenceph. Clin. Neurophysiol.*, **81,** 38–46.

PLONSEY, R. (1972) Capability and limitations of electrocardiography and magnetocardiography. *IEEE Trans.*, **BME-19,** 239–244.

PRESS, W. H., FLANNERY, B. P., TEUKOLSKY, S. A. and VETTERLING, W. T. (1986) *Numerical recipes.* Cambridge University Press, New York.

REILLY, J. P. (1989) Peripheral nerve stimulation by induced electric currents: exposure to time-varying magnetic fields. *Med. & Biol. Eng. & Comput.*, **27,** 101–110.

ROTH, B. J. and BASSER, P. J. (1990) A model of the stimulation of a nerve fiber by electromagnetic induction. *IEEE Trans.*, **BME-37,** 588–597.

ROTH, B. J., SAYPOL, J. M., HALLETT, M. and COHEN, L. G. (1991) A theoretical calculation of the electric field induced in the cortex during magnetic stimulation. *Electroenceph. Clin. Neurophysiol.*, **81,** 47–56.

SINGH, S., RICHARDS, W. F., ZINECKER, J. R. and WILTON, D. R. (1990) Accelerating the convergence of series representing the free space periodic Green's function. *IEEE Trans.*, **AP-38,** 1958–1962.

STOY, R. D., FOSTER, K. R. and SCHWAN, H. P. (1982) Dielectric properties of mammalian tissues from 0.1 to 100 MHz: a summary of recent data. *Phys. in Med. & Biol.*, **27,** 501–513.

TOFTS, P. S. (1990) The distribution of induced currents in magnetic stimulation of the nervous system. *Ibid.*, **35,** 1119–1128.

UENO, S., TASHIRO, T. and HARADA, K. (1988) Localized stimulation of neural tissues in the brain by means of a paired configuration of time-varying magnetic fields. *J. Appl. Phys.*, **64,** 5862–5864.

UENO, S., MATSUDA, T. and FUJIKI, M. (1990) Functional mapping of the human cortex obtained by focal and vectorial magnetic stimulation of the brain. *IEEE Trans.*, **MAG-26,** 1539–1544.

WILLIAMSON, S. J. and KAUFMAN, L. (1984) Frontiers in the new science of biomagnetism. In *Biomagnetism: applications & theory.* WEINBERG, H., STROINK, G. and KATILA, T. (Eds.), Pergamon Press, New York, 471–490.

Appendix

Because the second double summation in eqn. 23 is zero, the expansion coefficients of the potential function (eqn. 24) are independent of r_0, the radius of the sphere. This is the key condition that forces the steady-state radial electric field to be zero everywhere inside the sphere when a ramp current is applied to the excitation coil, and also greatly simplifies the expression for the total induced field. This Appendix shows that the second double summation of eqn. 23 is identically zero. The bracketed term in the second double summation of eqn. 23 can be expanded from the definitions given by eqns. 14 and 17:

$$\{\ \} = \oint_{\text{coil}} \frac{Y^*_{l+1,\,m-1}(\theta', \phi')}{2(2l+3)r'^{\,l+2}} \times \sqrt{\frac{(l-m+2)(l-m+1)}{(2l+1)(2l+3)}}\,(dx' - jdy') - \oint_{\text{coil}} \frac{Y^*_{l+1,\,m+1}(\theta', \phi')}{2(2l+3)r'^{\,l+2}} \times \sqrt{\frac{(l+m+2)(l+m+1)}{(2l+1)(2l+3)}}\,(dx' + jdy') + \oint_{\text{coil}} \frac{Y^*_{l+1,\,m}(\theta', \phi')}{(2l+3)r'^{\,l+2}} \times \sqrt{\frac{(l-m+1)(l+m+1)}{(2l+1)(2l+3)}}\,dz' \tag{29}$$

Eqn. 29 can be compactly written as

$$\{\ \} = \oint_{\text{coil}} \boldsymbol{Q} \cdot d\boldsymbol{l}' \tag{30}$$

where

$$\boldsymbol{Q} = \frac{Y^*_{l+1,\,m-1}\sqrt{\frac{(l-m+2)(l-m+1)}{(2l+1)(2l+3)}} - Y^*_{l+1,\,m+1}\sqrt{\frac{(l+m+2)(l+m+1)}{(2l+1)(2l+3)}}}{2(2l+3)r'^{\,l+2}}\,\hat{\boldsymbol{i}} - j\frac{Y^*_{l+1,\,m-1}\sqrt{\frac{(l-m+2)(l-m+1)}{(2l+1)(2l+3)}} + Y^*_{l+1,\,m+1}\sqrt{\frac{(l+m+2)(l+m+1)}{(2l+1)(2l+3)}}}{2(2l+3)r'^{\,l+2}}\,\hat{\boldsymbol{j}} + \frac{Y^*_{l+1,\,m}}{(2l+3)r'^{\,l+2}}\sqrt{\frac{(l-m+1)(l+m+1)}{(2l+1)(2l+3)}}\,\hat{\boldsymbol{k}} \tag{31}$$

The θ' and ϕ' arguments of the spherical harmonic functions have been dropped for brevity. If the curl of eqn. 31 is zero, then $\boldsymbol{Q}$ can be found from the gradient of a scalar function:

$$\boldsymbol{Q} = \nabla\psi \tag{32}$$

It is easier to find the scalar function than to take the curl of eqn. 31:

$$\psi = -\frac{(-1)^m}{2l+3}\sqrt{\frac{(l-m)!}{4\pi(2l+1)(l+m)!}}\,\frac{e^{-jm\phi}}{r'^{\,l+1}} \times [P^m_{l+1}(\cos\theta)\cos\theta - (l-m+2)P^{m-1}_{l+1}(\cos\theta)\sin\theta] \tag{33}$$

where P^m_l is the associated Legendre polynomial. Note that the $(-1)^m$ phase factor is found in the spherical harmonic function normalisation, and not in the Legendre polynomial in eqn. 33. The bracketed term must be identically zero, because eqns. 30 and 32 show that it is a closed line integral around the gradient of a scalar function (a conservative field). If the currents cannot be treated as filaments, but are distributed over some finite volume of the coil, the bracketed term is still zero. This is easily shown by using eqns. 32 and 33 and applying Gauss' theorem to the resulting volume integral, integrating over a volume slightly larger than the coil.

Author's biography

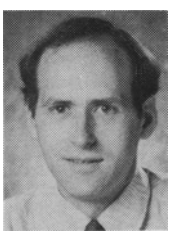

Harry A. C. Eaton received a BS degree from Colorado State University in 1985 and an MS degree from Johns Hopkins University in 1991, both in Electrical Engineering. From 1985 to 1988 he worked for the Applied Physics Laboratory's submarine technology test group designing various undersea instruments. He joined APL's Biomedical Programs Office in 1988 and is head of the Bioelectromagnetics Laboratory at APL. Mr Eaton is a member of Tau Beta Pi and the IEEE EMBS.